Unsteady Flow About Porous Cambered Shells

Turgut Sarpkaya* and Paul J. Lindsey†
Naval Postgraduate School, Monterey, California 93943

A numerical simulation was carried out through the use of the vortex-element methods to investigate the characteristics of an impulsively started uniform flow, decelerating at prescribed rates about a two-dimensional cambered porous shell, with an included angle of 120 deg, for the purpose of understanding the effects of porosity on the conditions under which wake recontact occurs.

Nomenclature

$4b$ = chord length of the cambered plate
C_d = drag coefficient, $D/(2\rho bU_0^2)$
C_p = pressure coefficient, $(2\Delta p/\rho V_n^2)^{1/2}$
c = radius of the circular cylinder
D = drag force per unit length
i = imaginary number
m = offset of the arc center in the circle plane
q = velocity vector
p = pressure
R = radius of the camber
$R\{\ \}$ = real part of a complex quantity
Re = Reynolds number, $4bU_0/\nu$
r = radial distance
T = normalized time
T^* = time at onset of deceleration
t = time
U = velocity
U = acceleration
U_0 = steady ambient velocity
U_s = velocity at separation point
u = x component of velocity
V_1 = tip velocity
V_2 = velocity at the inner edge of the shear layer
V_n = velocity normal to the camber
V_t = tangential velocity component
v = y component of velocity
w = complex potential function
z = $x+iy$, a point in the physical plane
z_n = location of the nth vortex
z_t = tip coordinate in the physical plane
Δt = time increment
Γ_n = circulation of the nth vortex
2α = included camber angle
β = porosity coefficient, $(0 \le \beta \le 1)$
δ = Rosenhead's smoothing parameter
ζ = $\xi+i\eta$, normalized location in circle plane
ζ_0 = nascent vortex position in circle plane
ζ_t = position of camber edge in circle plane
ζ_v = position of a vortex in circle plane
θ = counterclockwise angular position
θ_s = angular position of separation point
ν = kinematic viscosity
ρ = density of water

Received Sept. 25, 1989; presented as Paper 90-0314 at the AIAA 28th Aerospace Sciences Meeting, Reno, NV, Jan. 8–11, 1990; revision received Oct. 16, 1990; accepted for publication Oct. 16, 1990.

*Distinguished Professor of Mechanical Engineering, Code ME-SL. Associate Fellow AIAA.
†Lieutenant Commander, U.S. Navy.

Introduction

THE genesis of the investigation is the understanding of the reasons leading to the collapse of large parachutes and the effect of flow through the porous canopy on the prevention of the wake recontact phenomenon. Large parachutes have been observed to collapse during periods of rapid deceleration, subsequent to their initial inflation, with a resulting loss of drag and payload. Spahr and Wolf[1] noted that as the parachute assembly decelerates, the momentum in the wake is in some cases more than sufficient to cause the wake to overtake the canopy. The return of the wake to its generating body is a commonly encountered complex phenomenon in decelerating or oscillating flows.[2] Thus, the understanding of the physics of a passive control mechanism (blowing through a porous wall to push the wake away) for the prevention of wake recontact is of fundamental importance. It is with this realization that Sarpkaya et al.[3] have recently undertaken a numerical and experimental study of the separated time-dependent flow about two-dimensional rigid cambered shells, with included angles of 120, 180, and 240 deg, through the use of the vortex-element methods.[4] They have shown, among other things, that following the onset of deceleration and wake return, the differential pressure near the axis of the camber becomes increasingly negative. Had the model been flexible (as in the case of a parachute), the part of the canopy that first comes into contact with the wake would have collapsed as a result of the particular differential pressure to which it is subjected. Evidently, the collapsed shape would not have remained symmetrical (since the wake is normally asymmetrical), as evidenced by field experiments[1] with large axisymmetric parachutes.

It has long been recognized that the flow through the porous canopy, if managed properly, can help to minimize or eliminate the collapse phenomenon by eliminating the negative differential pressure across certain sections of the canopy. The present investigation was undertaken to study in detail the effect of porosity on a two-dimensional rigid, but porous, shell in order to bring the highly idealized problem a step closer to reality. In the following, the fundamental concepts used in the introduction of flow through a porous wall and the results obtained with various porosities through the use of the vortex-element methods are described in some detail.

Flow Through Porous Screens

The amount of flow through a porous material depends on the ratio of the open area; the shape, size, and elasticity of the threads; the moisture content of the material; the differential pressure across the canopy; the angle of approach of the ambient flow; and the magnitude, direction, and state of flows on the upstream and downstream faces of the wall.

In order to incorporate the effect of porosity into the analysis, one has to know at least the flow rate through the canopy as a function of the local differential pressure, assuming that the other parameters cited earlier are of secondary importance, or that their effects may be incorporated into a flow coefficient

relating differential pressure to the normal velocity of the flow rate. This seemingly simple search for a reliable (theoretical and/or experimental) equation is anything but simple. The following is a brief description of the previous investigations of flow through screens.

A fairly detailed review of the flow through screens is given by Laws and Livesey.[5] There are a number of investigations (see, e.g., Graham[6]) that have dealt with the flow past fairly porous screens for the purpose of understanding, managing, or generating isotropic turbulence. Often the resistance through the screen was of minor importance. Others (see, e.g., Taylor,[7] Taylor and Davies,[8] Wieghardt[9]) who examined the flow through infinite screens expressed the resistance as $\Delta p = \frac{1}{2}\rho K U^2$. Koo and James[10] and Cumberbatch[11] investigated the flow past finite screens set in infinite flows by replacing the screen with a source distribution and adjusting the stream function to yield the correct mass and momentum flux across the screen. However, the effects of body shape, flow separation, vortex formation, flow magnitude and direction downstream of the body, and deceleration of the flow were not investigated. It is clear that there is an enormous amount of research done on the flow through screens and yet there is very little information that could be extracted from this research for use in connection with a finite porous canopy. Payne[12] reviewed the data from many researchers in an effort to relate the geometric porosity (open area ratio) to the differential pressure and developed an equation in terms of a dynamic pressure loss term and a viscous loss term, as

$$\Delta p = K_1 U^2 + K_2 U$$

However valuable, this study did not deal with the effects of flow direction. This prompted the undertaking of an experimental investigation to establish the proper relationship between the pressure drop, the flow rate, and the flow direction on the actual samples of canopy materials used in parachutes.

The purpose of the experiments was twofold: to find the differential pressure vs flow rate relationship, and to find the variation, if any, of this relationship with the downstream flow direction. For this purpose, canopy samples were mounted smoothly on top of a rectangular opening on one of the walls of a small wind tunnel. A rectangular pipe (2 in. × 6 in. in cross section and 30 in. long, equipped with flow straighteners) was attached to the tunnel wall, directly in front of the opening, to blow measured amounts of air through the sample cloth. The pressures upstream and downstream of the screen were recorded for each flow rate through the screen and through the tunnel. Observations have shown that the canopy sample did not bulge measurably during the experiments, even at the differential pressures encountered by a parachute beginning to descend at a speed of about 600 mph (880 ft/s). This was primarily due to the proper construction and sandwiching of the circumference of the canopy sample to the tunnel wall. However, this is not meant to exclude the possibility that at high pressures the slight cambering of the sample may have stretched it and thereby increased its porosity slightly, leading to a relatively smaller differential pressure for a given flow rate. In fact, this was checked by conducting the experiments first with increasing and then decreasing flow rates. No attempt was made to wait a long time after the completion of the experiment with ascending pressures to see if the material would return to its original unstretched shape, or whether fibers used in the construction of the canopies would develop a permanent set beyond certain differential pressures and retain their deformed shape. This leads to the possibility that a once-used parachute may fall faster than a never-used one.

Of the seven available canopy materials, four samples were chosen and tested to provide a range of data. The characteristics of the four samples are shown in Table 1. The identifying letters are used for later reference.

During the course of the experiments, the flow on the downstream face of the sample was systematically changed to see if the differential pressure across the sample would increase for a given flow rate through the sample. The results of tests on the effect of flow on the downstream face of the samples have emphatically and somewhat surprisingly shown that the flow through the screens investigated is not affected by the presence or absence of the downstream flow. This apparently simple finding is of extreme mathematical and practical importance. It simplifies, for a first-order of approximation, the analysis and the possible management of porosity to minimize the consequences of wake recontact. It does not, however, resolve the more fundamental question regarding the effect of flow acceleration or deceleration on the flow through the screens.

The steady-flow results obtained with the four canopy samples have shown that[13] the pressure coefficient C_p, defined by

$$C_p = \sqrt{\frac{2\Delta p}{\rho V_n^2}}$$

remains nearly independent of velocity for a given canopy. Table 2 shows the minimum, mean, and maximum values of the pressure coefficient for the different samples.

Table 1 Characteristics of the canopy samples

			Military specification
A	Nylon	1.10 oz	None
B	Nylon	4.75 oz	(MIL-C-8021D-Type I)
C	Nylon	7.00 oz	(MIL-C-8021D-Type II)
D	Kevlar	3.00 oz	None

Table 2 Pressure coefficient for canopy samples

	C_p		
	Min.	Mean	Max.
A	20.3	22.9	27.3
B	33.0	36.7	43.0
C	39	42.8	48.9
D	61.5	66.3	73.3

Table 3 Geometrical relationships

		m	2α	b	$R = 1/m$
Model	A	0.500	120	0.866	2
Model	B	0.707	180	0.707	$\sqrt{2}$
Model	C	0.866	240	0.500	$2/\sqrt{3}$

Analysis

Conformal Transformations and Velocity Potential

The calculation of the velocity of any one of the vortices and the force acting on the body requires a conformal transformation (in which the camber becomes a circle), a complex velocity potential representing the vortices, their images, and the two dimensional irrotational flow around the body, and the use of the generalized Blasius theorem.

The flow in the circle plane (Fig. 1a) may be transformed to that about a cambered plate (Fig. 1b) through the use of

$$z = \zeta + m - \frac{b^2}{\zeta + m} + \frac{1 - 2m^2}{m} \tag{1}$$

It is to be noted for later use that $w = -\beta U z$ represents the velocity potential for a uniform flow of velocity βU past a porous shell in the z plane. Table 3 summarizes the relationships between m, α, b, and the radius of the camber.

The complex velocity potential w in the circle plane that describes the ambient flow U (assumed to be time dependent), Γ_{kq} clockwise-rotating vortices (called q vortices), Γ_{kp} coun-

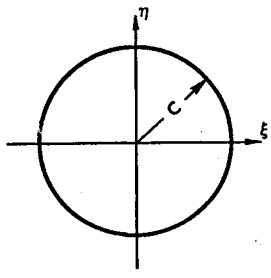

Fig. 1a Circle plane.

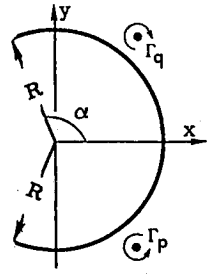

Fig. 1b Physical plane.

ter-clockwise-rotating vortices (called p vortices), and the images of all of the p and q vortices in the circle plane may be written as

$$w = -\beta U\left(\zeta + m - \frac{b^2}{\zeta+m} + \frac{1-2m^2}{m}\right) - (1-\beta)U\left(\zeta + \frac{c^2}{\zeta}\right) + \frac{i\Gamma_{0p}}{2\pi}\ln(\zeta-\zeta_{0p}) - \frac{i\Gamma_{0p}}{2\pi}\ln\left(\zeta - \frac{c^2}{\bar{\zeta}_{0p}}\right) + \sum\frac{i\Gamma_{kp}}{2\pi}\ln(\zeta-\zeta_{kp}) - \sum\frac{i\Gamma_{kp}}{2\pi}\ln\left(\zeta - \frac{c^2}{\bar{\zeta}_{kp}}\right) - \frac{i\Gamma_{0q}}{2\pi}\ln(\zeta-\zeta_{0q}) + \frac{i\Gamma_{0q}}{2\pi}\ln\left(\zeta - \frac{c^2}{\bar{\zeta}_{0q}}\right) - \sum\frac{i\Gamma_{kp}}{2\pi}\ln(\zeta-\zeta_{kq}) + \sum\frac{i\Gamma_{kq}}{2\pi}\ln\left(\zeta - \frac{c^2}{\bar{\zeta}_{kq}}\right) \tag{2}$$

in which Γ_{kp} and ζ_{kp} represent, respectively, the strength and location of the kth p vortex, Γ_{kq} and ζ_{kq} the strength and location of the kth q vortex, and c the radius of the cylinder; an overbar indicates a complex conjugate. The need for the separate identification of the p and q vortices and for the singling out of the nascent vortices in each shear layer (i.e., Γ_{0p} and Γ_{0q}) will later become clear.[3,14] The first term on the right side of the equation represents the velocity potential for a specified fraction β of the uniform flow U past through the camber (i.e., $-\beta Uz$), and the second term represents the potential for the flow going around the camber plus the doublet in the circle plane, as per circle theorem.

Complex Velocities of Vortices

The convection of the vortices and the calculation of the forces acting on the body require the evaluation of the velocities at the vortex centers in the physical plane. Using Routh's rule,[3,14] one has

$$-u_x + iv_y = \frac{\mathrm{d}}{\mathrm{d}\zeta}\left[w(\zeta) - \frac{i\Gamma}{2\pi}\ln(\zeta-\zeta_v)\right]\frac{1}{f'(\zeta)}\bigg|_{\zeta=\zeta_v} - \frac{i\Gamma}{4\pi}\frac{f''(\zeta_v)}{f'^2(\zeta_v)} \tag{3}$$

in which the last term in Eq. (3), for a p vortex, for example, reduces to

$$\frac{i\Gamma_{kp}}{4\pi}\frac{b^2(\zeta_{kp}+m)}{\left[(\zeta_{kp}+m)^2+b^2\right]^2} \tag{4}$$

Similar results may be obtained for other vortices.

The fact that the flow separates tangentially with a finite velocity at the edges of the camber (Kutta condition) may be expressed by requiring

$$\frac{\mathrm{d}w}{\mathrm{d}\zeta} = 0 \qquad \text{at } \zeta = \zeta_t = m \pm ib \tag{5}$$

Thus, inserting Eq. (2) in Eq. (5), one has

$$\frac{i\Gamma_{0p}}{2\pi}\left(\frac{1}{\zeta_t-\zeta_{0p}} - \frac{1}{\zeta_t-(c^2/\bar{\zeta}_{0p})}\right) - \frac{i\Gamma_{0q}}{2\pi}\frac{1}{\zeta_t-\zeta_{0q}} - \frac{1}{\zeta_t-(c^2/\bar{\zeta}_{0q})} + \sum\frac{i\Gamma_{kp}}{2\pi}\left(\frac{1}{\zeta_t-\zeta_{kp}} - \frac{1}{\zeta_t-(c^2/\bar{\zeta}_{kp})}\right) - \sum\frac{i\Gamma_{kq}}{2\pi}\left(\frac{1}{\zeta_t-\zeta_{kq}} - \frac{1}{\zeta_t-(c^2/\bar{\zeta}_{kq})}\right) - U\beta\left(1+\frac{b^2}{(\zeta_t+m)^2}\right) - U(1-\beta)\left(1-\frac{c^2}{\bar{\zeta}_t^2}\right) = 0 \tag{6}$$

Equation (6) may be decomposed into two parts as

$$\frac{i\Gamma_{0p}}{2\pi}\left(\frac{1}{\zeta_t-\zeta_{0q}} - \frac{1}{\zeta_t-(c^2/\bar{\zeta}_{0q})}\right) - \frac{i\Gamma_{0q}}{2\pi}\left(\frac{1}{\zeta_t-\zeta_{0q}} - \frac{1}{\zeta_t-(c^2/\bar{\zeta}_{0q})}\right) + (-U_{t0}+iV_{t0}) = 0 \tag{7}$$

where the terms containing the strength of the nascent vortices represent the velocity induced at the tip of the camber by the nascent vortices, and the term in parentheses, $(-U_{t0}+iV_{t0})$, represents the velocity at the tip due to flow *through* the camber, flow *around* the camber, doublet at the center of the circle in the ζ plane, and all of the wake vortices (and their images), excluding the nascent vortices.

Equation (7) represents two coupled equations for the strengths and positions of the nascent vortices. Thus, the solution of the said equations does, in general, require an iteration. However, this iteration may be avoided by noting that the velocity induced by a nascent vortex and its image at the opposite tip is very small and certainly negligible. Thus, Eq. (7), for one of the nascent vortices, may be reduced to

$$-\frac{i\Gamma_{0q}}{2\pi}\left(\frac{1}{\zeta_t-\zeta_{0q}} - \frac{1}{\zeta_t-(c^2/\bar{\zeta}_{0q})}\right) + (-U_{t0}+iV_{t0}) = 0 \tag{8}$$

A similar expression may be written for the other nascent vortex.

Flow Through the Porous Wall

The only analytical work that dealt only with *steady uniform* flow past a two-dimensional porous *plate* of width $4c$ (held normal to the flow) was carried out by Inoue.[16] The flow was started impulsively from rest at a constant velocity of U. Inoue made no attempt to relate the differential pressure across the plate to the flow rate. According to his method, the complex function for a plate normal to the flow is given, in our notation, by

$$w = -\beta U\left(\zeta - \frac{c^2}{\zeta}\right) - U(1-\beta)\left(\zeta + \frac{c^2}{\zeta}\right) + \sum\frac{i\Gamma_{kp}}{2\pi}\ln(\zeta-\zeta_{kp}) - \sum\frac{i\Gamma_{kp}}{2\pi}\ln\left(\zeta - \frac{c^2}{\bar{\zeta}_{kp}}\right) - \sum\frac{i\Gamma_{kq}}{2\pi}\ln(\zeta-\zeta_{kq}) + \sum\frac{i\Gamma_{kq}}{2\pi}\ln\left(\zeta - \frac{c^2}{\bar{\zeta}_{kq}}\right) \tag{9}$$

in which β $(0 \le \beta \le 1)$ is an artificial porosity coefficient. The first term on the right side of Eq. (9) represents the contribution of the uniform flow βU, the second term represents the potential flow around a plate of width $4c$, and the remaining terms represent the contributions of the discrete vortices (including the nascent vortices). Clearly, βU is the uniform part of the flow that passes through the screen, regardless of the differential pressure distribution prevailing along the screen. Inoue did not examine the pressure distribution along the plate and confined himself to the comparison of the calculated flow

kinematics with sample flow pictures, presumably obtained under conditions similar to those encountered in the numerical calculations. Thus, his results correspond to screens with nonuniform and unknown porosity distributions.

Computational Details

With the realization of the fact that the flow through the camber must be related to the prevailing differential pressure and that the direction of the flow in the wake has no measurable effect on the differential pressure vs dynamic head, a new method had to be devised that would properly account for the effect of porosity.

The present method takes advantage of the simplicity of Inoue's method and accounts for the local dependence of the flow on differential pressure. For this purpose, the value of β is chosen (e.g., $\beta = 0.25$) so as to make V_n at $\theta = 0.0$ proportional to $\sqrt{\Delta p}$. The variations in the flow across the camber beyond and above that given by Inoue's method are accounted for through the use of discrete vortices placed along the camber. A number of sample calculations have shown that the use of 118 body vortices (one every degree) on a 120-deg camber will be more than sufficient to account for the additional cross-flow effects smoothly. The first vortices were placed one degree from the tips, and no vortex was placed at $\theta = 0$. The midpoints between the vortices were used as the control points to calculate the velocity normal to the camber. At each control point, the differential pressure was calculated,[3,15] and then V_n was found from

$$V_n = \frac{1}{C_p}\sqrt{\frac{2\Delta p}{\rho}} \tag{10}$$

for a given C_p (see Table 2). The normal component of the velocity induced by the uniform flow based on β was subtracted, and then the strengths of the body vortices were determined by equating the remaining velocity to that induced by the body vortices at the control points. Once the strengths of the body vortices were determined, the velocity induced at each vortex in the wake was calculated, the velocity of the ambient flow was updated, and all of the wake vortices were convected for a time interval Δt using a second-order modified Eulerian scheme. The procedure was then repeated, up to any specific time (in this analysis $T = 25$). The method of introduction of the nascent vortices has been described in detail by Sarpkaya et al.[3] and will not be repeated here. Suffice it to note that in the present calculations only the constant-Δt method rather than the variable-Δt method was used. The wake vortices were never merged together, no matter how close they came, and were only removed from the simulation if they contacted the camber. To prevent abnormally high induced velocities from occurring due to the proximity of one vortex to another, whether body or wake vortices, Rosenhead's[17] smoothing scheme was used, i.e., the complex velocity at a point was multiplied by

$$\frac{|z_k - z_j|^2}{|z_k - z_j|^2 + \delta^2} \tag{11}$$

where $|z_k - z_j|$ is the distance between the vortex centers and δ is the attenuation factor. In this analysis, δ was chosen to be 0.05. A detailed discussion of Rosenhead's scheme is given by Sarpkaya.[4]

The method described above is quite general and could be used to investigate the effect of porosity on any canopy. Because it was deemed sufficient to explore the physics of the phenomenon, only two porosities were used in the numerical experiments. The first corresponded to the characteristics of the canopy sample A ($C_p = 22.9$, with $\beta = 0.045$, see Table 2), and the second to a canopy that is much more porous than any of the samples tested, with an assumed $C_p = 4.45$, which required an initial value of $\beta = 0.25$ at $T = 0.5$ at $\theta = 0$.

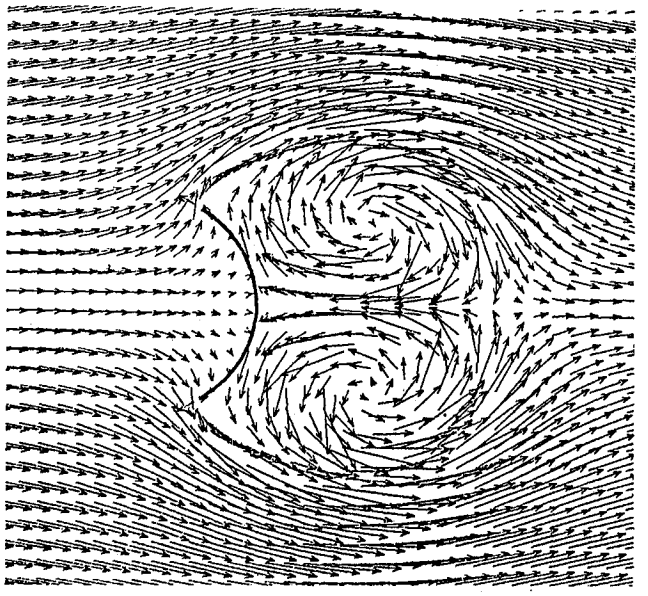

Fig. 2a Flow about a 120-deg cambered shell at $T = 8.64$ ($C_p = 22.9$ and $b = 0.049$).

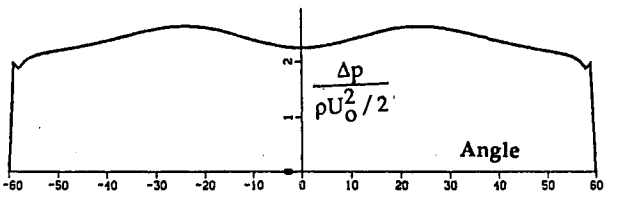

Fig. 2b Differential pressure distribution at $T = 8.64$ ($C_p = 22.9$ and $b = 0.049$).

Discussion of Results

The numerical experiments were carried out for a number of time-dependent normalized velocities, chosen on the basis of the physical experiments carried out in a vertical water tunnel with nonporous cambers.[3,15] The variations of velocity and acceleration with time were either represented by suitable functions or left in digitized form for use in the calculations. A sample velocity history is given by

$$0 \le T \le 10, \qquad V_R = 1 \tag{12a}$$

$$10 < T^* < 18, \qquad V_R = 0.5 + 0.5\cos\left[0.125\pi(T - 10)\right] \tag{12b}$$

$$T \ge 18, \qquad V_R = 0, \qquad \frac{dV_R}{dt} = 0, \qquad U = U_t \tag{12c}$$

where

$$V_R = \frac{U - U_t}{U_0 - U_t} \quad \text{and} \quad T = \frac{(U_0 - U_t)t}{c} \tag{12d}$$

Clearly, Eq. (12a) assumes that the flow is accelerated impulsively from rest to a constant velocity. In general, this is not possible, and the measured and calculated forces differ at small times because of the differences between the measured and assumed initial acceleration histories.[3,15] Suffice it to note that, other than numerical experiments, there is no mechanical or traveling-shock system capable of generating a truly impulsive flow. Efforts to generate impulsive or uniformly accelerated flow at high Reynolds numbers or accelerations in a liquid medium are hampered by the generation of compression and rarefaction waves and regions of intense cavitation. These are some of the difficulties of the experiments with impulsive flows.

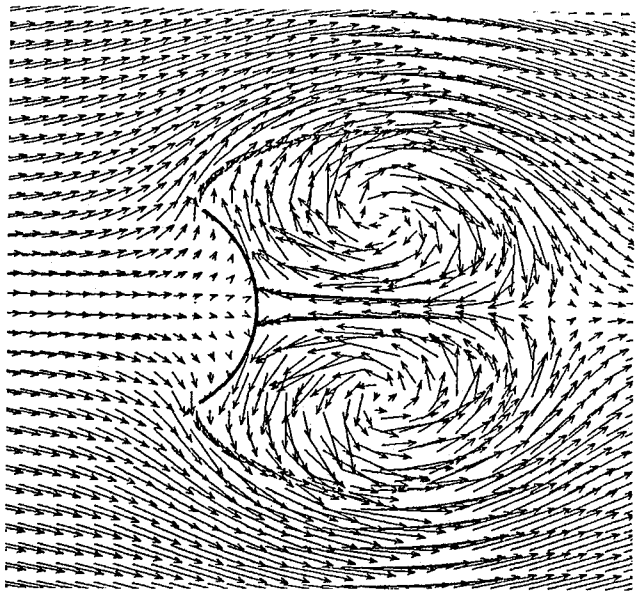

Fig. 3a Flow about a 120-deg cambered shell at $T = 11.29$ ($C_p = 22.9$ and $b = 0.049$).

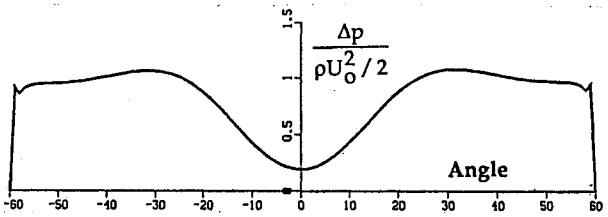

Fig. 3b Differential pressure distribution at $T = 11.29$ ($C_p = 22.9$ and $b = 0.049$).

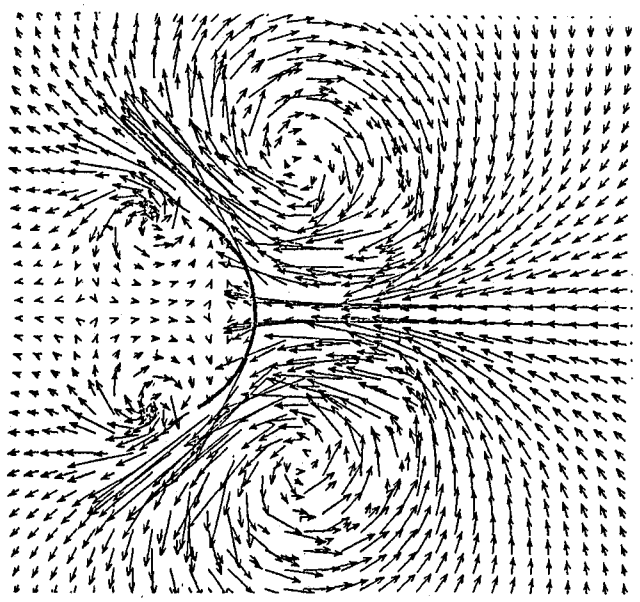

Fig. 4a Flow about a 120-deg cambered shell at $T = 15.36$ ($C_p = 22.9$ and $b = 0.049$).

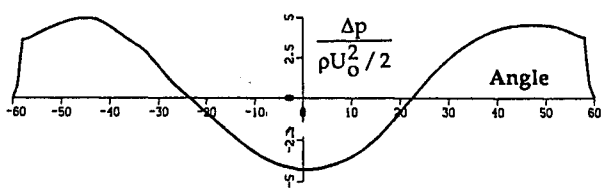

Fig. 4b Differential pressure distribution at $T = 15.36$ ($C_p = 22.9$ and $b = 0.049$).

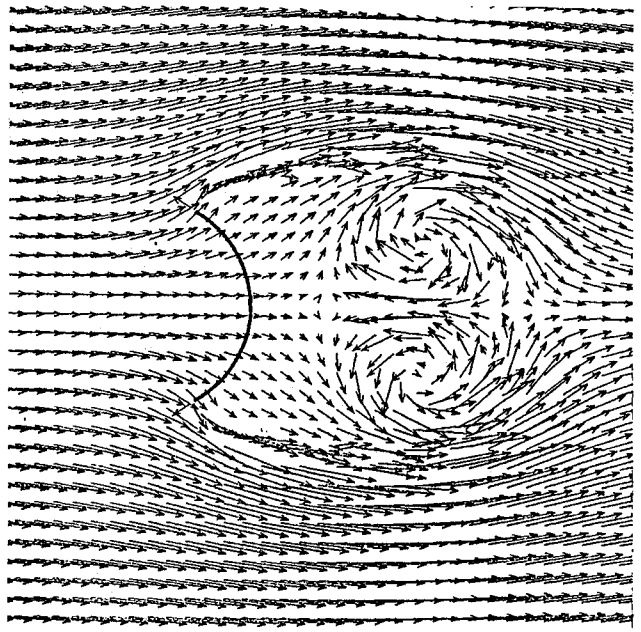

Fig. 5a Flow about a 120-deg cambered shell at $T = 8.64$ ($C_p = 4.45$ and $b = 0.25$).

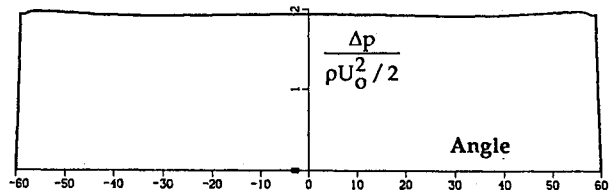

Fig. 5b Differential pressure distribution at $T = 8.64$ ($C_p = 4.45$ and $b = 0.25$).

Equations (12a–12d) require the specification of the initial velocity U_0 and the terminal velocity U_t or U_t/U_0. In general, the fall-velocity history of a given parachute depends on numerous parameters, such as the mass of the parachute system, physical characteristics of the ambient medium (air density, temperature, and viscosity), a characteristic diameter of the parachute, physical characteristics of the canopy (e.g., configuration, porosity distribution), gravitational acceleration, and the magnitude and direction of the initial velocity. Thus, one cannot arbitrarily specify the velocity history. Clearly, the instantaneous position of the wake relative to a given canopy (wake recontact) depends not only on the initial velocity and the rate of deceleration of the parachute but also on the duration of the deceleration or on the amount of reduction in the fall velocity, i.e., on U_t/U_0. Nevertheless, the understanding of the physics of the wake recontact problem may be enhanced through the use of a sufficiently realistic and yet relatively idealized velocity history. It is with this objective in mind that Eqs. (12a–12d) were used in the calculations. Even though the velocity ratio U_t/U_0 was varied systematically, only the results obtained with $U_t/U_0 = 1/6$ are reported herein.

Figures 2–4 show the evolution of the wake and the differential pressure distribution at times $T = 8.64$, 11.29, and 15.36 for $C_p = 22.9$ and $\beta = 0.049$ (sample A). The comparison of these figures with those presented by Sarpkaya et al.[3,15] for the nonporous case shows that the effect of porosity, however noticeable, is not large enough to produce a significant downstream displacement of the wake vortices. The importance of this conclusion lies in the fact that even the most porous parachute canopy used by the industry is not sufficiently porous to minimize the consequences of the wake return for certain combinations of the governing parameters, as evidenced by the field experiments.[1]

The next step in the analysis was to show the beneficial effects of porosity when it can be made sufficiently large. Figures 5–7 show the evolution of the wake and the differential pressure distribution at times $T=8.64$, 11.29, and 15.36 for $C_p=4.45$ and $\beta=0.25$. It is evident from a comparison of Figs. 2a, 3a, and 4a with Figs. 5a, 6a, and 7a that the wake is significantly displaced downstream and that, as seen in Figs. 5b, 6b, and 7b, the differential pressure $2\Delta p/\rho U_0^2$ (i.e., the pressure inside the camber minus the pressure outside) is less negative than those shown in Figs. 2b, 3b, and 4b. Figure 8 shows the evolution with time of the differential pressure at $\theta=0$ for the porous ($C_p=22.9$, $C_p=4.45$) and nonporous cases.[3,15] It is seen that the case of $C_p=22.9$ has differential pressures only slightly less in magnitude than the nonporous case, whereas the more porous case ($C_p=4.45$) has significantly smaller differential pressures. In other words, the effect of flow through the porous wall is to increase the base pressure.

Figure 9 shows the drag coefficient as a function of T for the two porosities cited earlier. Apparently, for $C_p=0.049$, not only the differential pressure at $\theta=0$ but also the net force acting on the entire camber becomes negative at some time during the course of the evolution of flow. For the case with $C_p=4.45$, the deceleration of flow brings, as expected, a gradual decrease in C_d, followed by an increase that reaches its maximum toward the end of the deceleration period. Nevertheless, the drag remains positive even though the differential pressure at $\theta=0$ goes through negative values. For $T>18$, however, the wake continues to approach the camber because of the mutual induction of the counter-rotating vortices on both sides of the camber, and C_d decreases once again, but only temporarily. Subsequently, the drag recovers, primarily due to the combined effects of the terminal velocity and the wall bleeding. At larger times, the drag coefficient is expected to oscillate about a mean value. The comparison of the two drag curves also shows that the effect of the larger porosity is partly to delay the decreases in C_d and partly to attenuate the oscillations superimposed on it. Apparently, flow through the porous canopy can substantially modify the wake and delay or inhibit the occurrence of negative differential pressures. However, the porosity required to achieve the desired result may be at the expense of reduced drag or increased terminal velocity. It is clear that the wake structure modification to inhibit para-

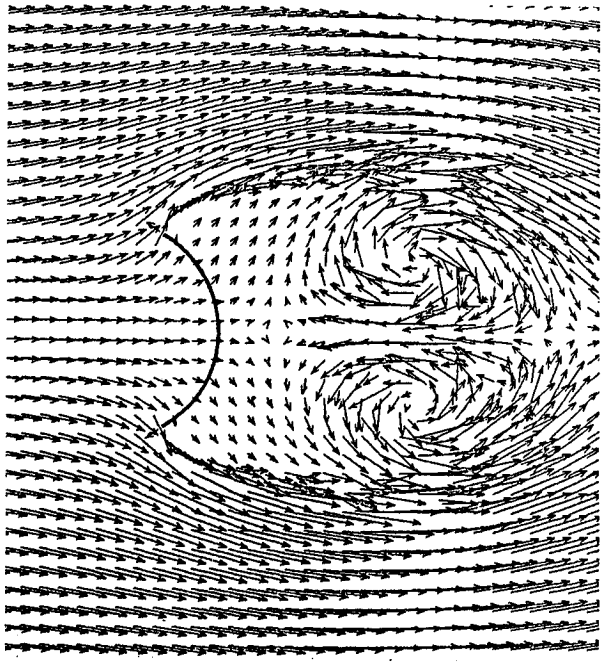

Fig. 6a Flow about a 120-deg cambered shell at $T=11.29$ ($C_p=4.45$ and $b=0.25$).

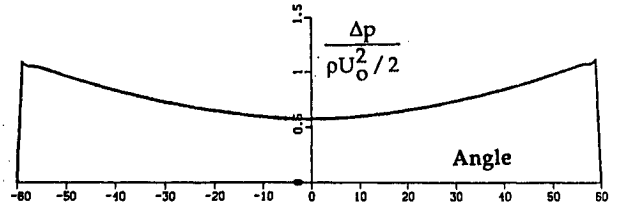

Fig. 6b Differential pressure distribution at $T=11.29$ ($C_p=4.45$ and $b=0.25$).

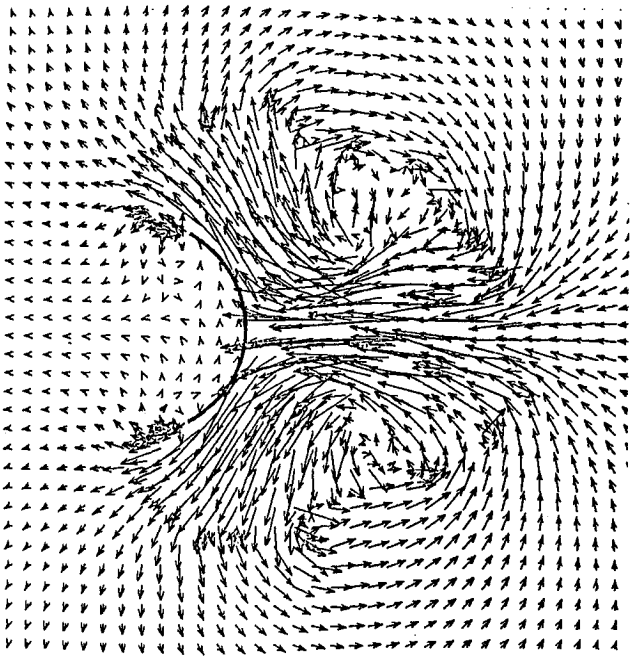

Fig. 7a Flow about a 120-deg cambered shell at $T=15.36$ ($C_p=4.45$ and $b=0.25$).

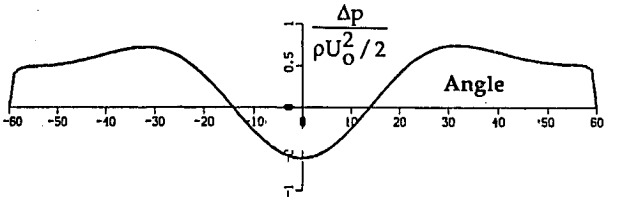

Fig. 7b Differential pressure distribution at $T=15.36$ ($C_p=4.45$ and $b=0.25$).

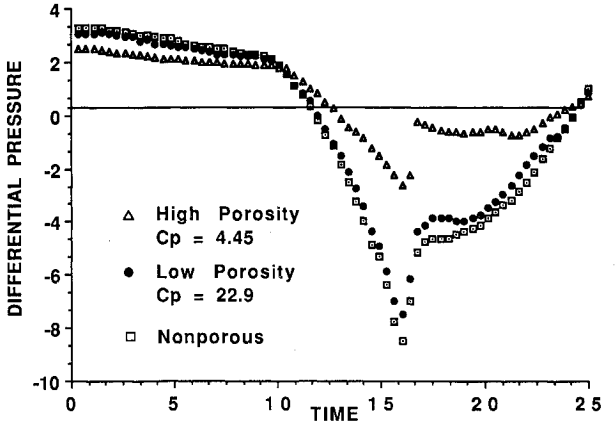

Fig. 8 Differential pressure $q=0$ as a function of time for various porosities.

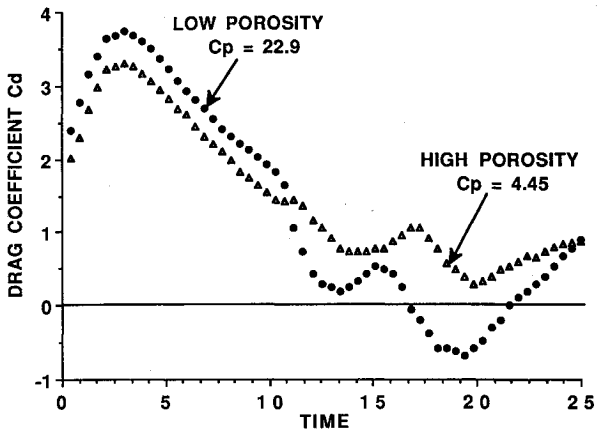

Fig. 9 C_d **vs time for high** ($C_p = 4.45$, $b = 0.25$) **and low** ($C_p = 22.9$, $b = 0.049$) **porosities.**

chute collapse should be achieved partly through modifications to the geometrical configuration and partly through the use of nonuniform porosity. The relatively idealized calculations presented herein also suggest that both U_t/U_0 and the normalized distance s/D covered by the parachute *during its deceleration period* should be made as large as practically possible to minimize wake recontact.

Conclusions

A numerical investigation of an impulsively started steady uniform flow, decelerating at prescribed rates to another steady state, about a two-dimensional cambered porous shell with an included angle of 120 deg has been carried out using the vortex-element methods. The results have shown the following.

1) Initially, two highly stable symmetrical vortices form and continue to grow, giving rise to relatively large drag forces. During the period of deceleration, however, the vortices move toward the camber and give rise to regions of negative differential pressure and even to negative drag forces, depending on the intensity and duration of the deceleration and the magnitude of flow through the porous wall. Had the model been flexible (as in the case of a parachute), the central part of the camber would have collapsed as a result of the particular deceleration it is subjected to.

2) For cambers with relatively small porosities, the pattern of vortex shedding is much the same as that for rigid cambers. A small downstream motion of the vortex pair is discernible, but no striking changes take place. The effect of the increased porosity, however, is to move the vortex pair markedly downstream and attenuate and delay the consequences of the flow deceleration relative to the less porous case. Nevertheless, it is possible to find deceleration rates and U_t/U_0 values for which strong wake recontact and parachute collapse will take place regardless of the degree of porosity (within practical limits, of course, without substantial or unacceptable sacrifice in terminal velocity).

3) Flow through a porous body should be regarded as one of the passive means to modify the structure, as well as the behavior of the wake of a body undergoing rapid deceleration. Other forms of wake manipulation need to be explored in addition to the use of increased porosity. The results of the numerous calculations with other rates of deceleration and U_t/U_0 ratios suggest that both U_t/U_0 and the relative distance s/D covered by a parachute during its deceleration period should be made as large as possible in order to minimize the occurrence of negative differential pressures along the canopy.

4) The type of wake modification explored in this work needs to be pursued further in order to incorporate into the analysis the flexibility of the canopy. Furthermore, physical experiments with rigid as well as flexible screens (with variable porosities) or with actual canopy samples will provide an excellent opportunity to improve the predictions of the numerical method used.

5) Fast numerical experiments can be carried out with the model developed herein. It would have been extremely difficult, if not impossible, to achieve similar results with space discretization methods, within comparable CPU times. Thus, the investigation reported herein shows the power as well as the limitations of the vortex-element methods through the use of a highly complex separated time-dependent flow.

Acknowledgments

This paper was prepared in conjunction with research conducted for the Chief of Naval Research and funded by the Naval Postgraduate School. The senior author wishes to express his appreciation to James H. Strickland for arousing his interest in parachute collapse. The assistance provided by Jack McKay during the experiments leading to various deceleration histories is gratefully acknowledged.

References

[1]Spahr, H. R., and Wolf, D. F., "Theoretical Analysis of Wake-Induced Parachute Collapse," AIAA Paper 81-1922, Oct. 1981.

[2]Sarpkaya, T., and Isaacson, M., *Mechanics of Wave Forces on Offshore Structures,* Van Nostrand Reinhold, New York, 1981, p. 690.

[3]Sarpkaya, T., Mostafa, S. I. M., and Munz, P. D., "Numerical Simulation of Unsteady Flow About Cambered Plates," *Journal of Aircraft*, Vol. 27, No. 1, 1990, pp. 51–59.

[4]Sarpkaya, T., "Computational Methods with Vortices—The 1988 Freeman Scholar Lecture," *Journal of Fluids Engineering, Transactions of the American Society of Mechanical Engineers,* Vol. 111, No. 1, 1989, pp. 5–52.

[5]Laws, E. M., and Livesey, J. L., "Flow Through Screens," *Annual Review of Fluid Mechanics*, Vol. 10, 1978, pp. 247–266.

[6]Graham, J. M. R., "Turbulent Flow Past a Porous Plate," *Journal of Fluid Mechanics,* Vol. 73, Pt. 3, 1976, pp. 565–591.

[7]Taylor, G. I., "Air Resistance of a Flat Plate of Very Porous Material," *Scientific Papers of Sir Geoffrey Ingram Taylor*, edited by G. K. Batchelor, University Press, Cambridge, England, UK, Vol. 3, 1944, pp. 383–386.

[8]Taylor, G. I., and Davies, R. M., "The Aerodynamics of Porous Sheets," *Scientific Papers of Sir Geoffrey Ingram Taylor*," edited by G. K. Batchelor, University Press, Cambridge, England, UK, Vol. 3, 1944, pp. 391–405.

[9]Wieghardt, K. E. G., "On the Resistance of Screens," *Aeronautical Quarterly*, Vol. 4, 1953, pp. 186–192.

[10]Koo, J.-K., and James, D. F., "Fluid Flow Around and Through a Screen," *Journal of Fluid Mechanics*, Vol. 60, Pt. 3, 1973, pp. 513–538.

[11]Cumberbatch, E., "Two-Dimensional Flow Past a Mesh," *Quarterly Journal of Mechanics and Applied Mathematics*, Vol. 35, Pt. 3, 1982, pp. 335–344.

[12]Payne, P. R., "The Theory or Fabric Porosity as Applied to Parachutes in Incompressible Flow," *Aeronautical Quarterly*, Vol. 29, Pt. 3, 1978, pp. 175–206.

[13]Lindsey, P. J., "Unsteady Flow Past Porous Cambered Plates," M.S. Thesis, Naval Postgraduate School, Monterey, CA, June 1988.

[14]Sarpkaya, T., "An Inviscid Model of Two-Dimensional Vortex Shedding for Transient and Asymptotically Steady Separated Flow Over an Inclined Flat Plate," *Journal of Fluid Mechanics*, Vol. 68, 1975, pp. 109–128.

[15]Sarpkaya, T., Mostafa, S. I. M., and Munz, P. D., "Unsteady Flow about Cambered Plates," Naval Postgraduate School, Monterey, CA, TR NPS-69-87-012, Oct. 1987.

[16]Inoue, O., "A New Approach to Flow Problems Past a Porous Plate, *AIAA Journal,* Vol. 23, No. 12, 1985, pp. 952–958.

[17]Rosenhead, L., "The Spread of Vorticity in the Wake Behind a Cylinder," *Proceedings of the Royal Society,* Vol. 127, 1930, pp. 590–612.